

Surface Fluctuations and the Stability of Metal Nanowires

C.-H. Zhang,¹ F. Kassubek,² and C. A. Stafford¹

¹*Department of Physics, University of Arizona, 1118 E. 4th Street, Tucson, AZ 85721*

²*ABB Schweiz AG, Corporate Research, CH-5405, Baden-Dättwil, Switzerland*

(Dated: March 22, 2022)

The surface dynamics and thermodynamics of metal nanowires are investigated in a continuum model. Competition between surface tension and electron-shell effects leads to a rich stability diagram, with fingers of stability extending to extremely high temperatures for certain magic conductance values. The linearized dynamics of the nanowire's surface are investigated, including both acoustic surface phonons and surface self-diffusion of atoms. On the stability boundary, the surface exhibits critical fluctuations, and the nanowire becomes inhomogeneous. Some stability fingers coalesce at higher temperatures, or exhibit overhangs, leading to reentrant behavior. The nonlinear surface dynamics of unstable nanowires are also investigated in a single-mode approximation. We find evidence that some unstable nanowires do not break, but rather neck down to the next stable radius.

PACS numbers: 68.35.Ja, 47.20.Dr, 61.46.+w, 68.65.La

I. INTRODUCTION

Metal wires play an essential role in all electrical circuits, from power distribution between cities to interconnects in integrated circuits. In today's technology, feature sizes down to approximately 100nm are the state of the art, but current trends,¹ consistent with *Moore's law*,² extrapolate to 1nm technology by 2020. A question of fundamental importance is whether metal will retain its role as the conductor of choice even at the ultimate limit of atomic-scale technology, or whether it must be replaced with more exotic conductors, such as carbon nanotubes.³

A macroscopic analysis of the mechanical properties of thin metal wires suggests that it might be difficult to fabricate wires thinner than a few thousand atoms in cross section: Consider a cylindrical wire of radius R and length L . The maximum tension that the wire can sustain before the onset of plastic flow is $F_Y = \pi R^2 \sigma_Y$, where σ_Y is the *yield strength*. On the other hand, the force due to the surface tension σ_s in a thin wire is $F_s = -\pi R \sigma_s$. If $|F_s| > F_Y$, one would expect the wire to undergo plastic flow and, if $L > 2\pi R$, to break up under surface tension, as in the *Rayleigh instability* of a column of fluid.⁴ This estimate gives a minimum radius for solidity, $R_{\min} = \sigma_s / \sigma_Y$. The parameters for several simple metals are given in Table I. Plateau realized as early as 1873 that this surface-tension driven instability of a cylinder is unavoidable if cohesion is due solely to classical pairwise interactions between atoms.⁵

A great deal of experimental evidence has accumulated over the past decade, however, indicating that metal nanowires considerably thinner than the above estimate can be fabricated by a number of different techniques.^{11,12,13,14,15,16,17,18} Even wires with lengths significantly exceeding their circumference were found to be remarkably stable,^{13,14,17} indicating that some new

mechanism must intervene to prevent their breakup.

An important technique which has been used to model the energetics of metal nanowires is classical molecular dynamics,^{19,20,21,22,23,24} which utilizes short-ranged interatomic potentials optimized to fit the bulk properties of solids. This technique has had considerable success, including predicting the formation of metal nanocontacts in STM experiments¹⁹ and predicting novel, non-crystalline order in nanowires.²² However, this approach, which neglects quantum-size effects, is unable to avoid the Rayleigh instability in long wires.^{22,23,24}

A clue to the resolution of this problem was provided by the observation of electron-shell structure in conductance histograms of alkali metal nanocontacts.¹⁵ Like the surface tension, quantum-size effects arising from the confinement of the conduction electrons within the cross-

Metal	σ_Y (MPa)	σ_s (N/m)	$\sigma_s(\text{FEM})$ (N/m)	γ_s (pN)	$\gamma_s(\text{FEM})$ (pN)	σ_s/σ_Y (nm)	G_{\min} (G_0)
Cu	210	1.5	0.83	190	140	7.1	2300
Ag	140	1.0	0.51	154	95	7.4	1900
Au	100	1.3	0.51	257	96	13	5600
Li	15	0.44	0.37	99	75	29	26000
Na	10	0.22	0.17	39	41	22	10000

TABLE I: The yield strength σ_Y ,⁶ surface energy σ_s ,⁷ and curvature energy γ_s ⁸ of various monovalent metals. The values^{9,10} in the free-electron model, $\sigma_s(\text{FEM}) = \varepsilon_F k_F^2 / 80\pi$ and $\gamma_s(\text{FEM}) = 4\varepsilon_F k_F / 45\pi^2$, are shown for comparison. For a wire of radius $R < \sigma_s / \sigma_Y$, the stress due to surface tension exceeds σ_Y , signalling a breakdown of macroscopic elasticity theory. The electrical conductance G_{\min} of a ballistic wire of radius $R_{\min} = \sigma_s / \sigma_Y$ is shown in the rightmost column, in units of the conductance quantum $G_0 = 2e^2/h$. Note that G/G_0 is approximately equal to the number of atoms that fit within the cross section for monovalent metals.

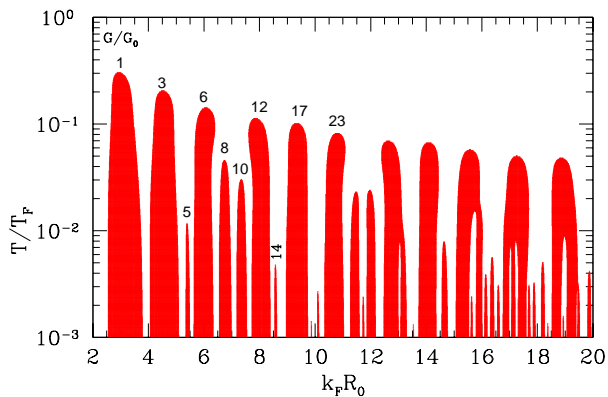


FIG. 1: Stability of cylindrical metal nanowires as a function of radius and temperature. Shaded regions indicate stability with respect to small perturbations, $A(R_0, T) > 0$; unshaded regions denote unstable configurations, $A(R_0, T) < 0$. Here T_F is the Fermi temperature, k_F the Fermi wavevector, and R_0 the mean radius of the wire. The quantized conductance values of some of the stable wires are indicated.

section of the wire become increasingly important as the wire is scaled down to atomic dimensions. In fact, a linear stability analysis²⁵ of metal nanowires within the free-electron model found that the Rayleigh instability can be completely suppressed for certain favorable radii.

In this article, we investigate the surface dynamics and thermodynamics of simple metal nanowires in a continuum approach, in order to shed further light on their unusual stability properties. The starting point for our analysis is the thermodynamic stability diagram shown in Fig. 1. Competition between surface tension and electron-shell effects leads to a complex landscape of stable fingers and arches extending up to very high temperatures: wires whose electrical conductance is a magic number 1, 3, 6, 12, 17, 23,... times the conductance quantum $G_0 = 2e^2/h$ are predicted to be stable with respect to small perturbations up to temperatures well above the bulk melting temperature $T_M \approx .01T_F$, where T_F is the Fermi temperature. This finding suggests that metal nanowires may be remarkably robust, which is cause for optimism about their potential for nanoelectronics applications.²⁶ Fig. 1 is akin to a *phase diagram* for metal nanowires; the nature of the different phases is revealed in this article through a study of the surface dynamics for small perturbations about a cylinder. We find that the stable fingers correspond to homogeneous (i.e., translationally invariant) phases, while the intervening regions correspond to inhomogeneous phases.

II. THE MODEL

The continuum model we employ allows for an analytical treatment of the long-wavelength surface modes used to characterize the different phases in Fig. 1, as well as a correct treatment of quantum-size effects, which

are essential to stabilize long nanowires. The ionic degrees of freedom of the wire are modeled as an incompressible, irrotational fluid, and the conduction electrons are treated as a Fermi gas confined within the wire by Dirichlet boundary conditions at the surface. Electron-electron interactions are included only at a macroscopic level (by requiring the wire to be electrically neutral), since it is well known^{9,10,27} that the leading mesoscopic shell-correction to the energy is independent of interactions. Calculations including interactions at the mean-field level^{28,29} yield shell effects very similar to those in the free-electron model.^{9,30}

Modelling the ionic degrees of freedom as a fluid is motivated by the argument presented in Table I, which indicates that metal nanowires thinner than a few thousand atoms in cross section should be very plastic. The free-electron model for the conduction electrons is appropriate to describe electron-shell effects in monovalent metals, and as the values in Table I indicate, even describes some macroscopic properties of alkali metals semi-quantitatively. Although the continuum approximation is not justified *a priori* in the limit of atomically-thin wires, this model is nonetheless justified *a posteriori* by its success in describing simple metal clusters³¹ of comparable dimensions. Cohesion and quantum transport in gold nanocontacts were also successfully described with this model.^{30,32,33} The directionality of bonding due to contributions from *p*-, *d*- and *f*-electrons is of course absent from the free-electron model, as are element-specific effects, such as the tendency toward surface reconstruction, which was argued to play an essential role in the formation of atomic chains.³⁴ Nonetheless, wires with $G = G_0$ are predicted to be very stable within the free-electron model, and the strength of a metallic bond in such a wire is significantly greater than that in the bulk.^{9,30}

An empirical justification for our continuum model comes from experimental results indicating that electron-shell effects dominate over ionic ordering in sufficiently thin alkali metal¹⁶ and gold¹⁸ wires. Yanson *et al.*¹⁶ found an interesting interplay between electron-shell effects and atomic-shell effects in alkali metal nanocontacts. Electron-shell effects were found to be most important in the lighter elements lithium and sodium, presumably due to the larger Fermi energies of the conduction electrons and the lighter, more mobile ions, while atomic-shell effects were most important in the heavier element potassium. A crossover from electron-shell structure to atomic-shell structure in conductance histograms was found for conductance values $G/G_0 \approx 36$ in potassium, while electron-shell effects were found to dominate even for $G/G_0 > 100$ in lithium. An intermediate behavior was observed for sodium. Interestingly, the competition between the two effects was found to be history dependent. In a particular sequence of histograms obtained by cycling a potassium break junction, an evolution from atomic-shell structure to electron-shell structure was observed.¹⁶ Most recently, a similar interplay

between electron-shell structure and atomic-shell structure was also observed in gold nanocontacts.¹⁸

These fascinating experimental results cry out for deeper theoretical investigations of the stability and structure of metal nanowires. While the geometry of the nanowires studied in Refs. 15,16,18 was not directly determined, they may be rather short due to the fabrication method, so that the connection³⁵ to the contacts may play an important role. In this article, we study the more theoretically tractable—and more technologically relevant—problem of the stability and surface dynamics of long metal nanowires. Our analysis should be directly relevant for the nanowires studied in Refs. 13,17.

III. LINEAR STABILITY ANALYSIS

In our continuum model, the ionic degrees of freedom are completely determined by the surface coordinates of the wire. Motivated by the fact that only modes which preserve axial symmetry participate in the surface-tension driven instability of a cylinder,⁴ we restrict our consideration to axially-symmetric perturbations,

$$R(z, t) = R_0 + \sum_n b(q_n, t) e^{iq_n z}, \quad (1)$$

where $R(z, t)$ is the radius of the wire at position z and time t , R_0 is the unperturbed radius, and $b(q, t) = b^*(-q, t)$ are complex Fourier coefficients. Periodic boundary conditions are assumed for a wire of length L , so that $q_n = 2\pi n/L$, with n an integer bounded by $|n| \leq N \approx k_F L/\pi$ (a lattice cutoff). Since the total number of atoms comprising the nanowire is unchanged by the perturbation, $b(0, t)$ is related to the other $b(q_n, t)$ by volume conservation

$$b(0, t) + \frac{b^2(0, t)}{2R_0} = -\frac{1}{R_0} \sum_{n=1}^N |b(q_n, t)|^2, \quad (2)$$

and may be eliminated.

For small perturbations, the grand canonical potential of the electron gas is quadratic in the Fourier coefficients $b(q, t)$, and determines the potential energy U of the ions in the Born-Oppenheimer approximation,

$$U = U_0(R_0, T) + L \sum_{n=1}^N \alpha(q_n; R_0, T) |b(q_n, t)|^2, \quad (3)$$

where $U_0(R_0, T)$ is the potential energy of an unperturbed cylinder,

$$\frac{U_0(R, T)}{L} = \pi R^2 u + 2\pi R \sigma_s - \pi \gamma_s + V(R, T). \quad (4)$$

Here u is the macroscopic free energy density of the electron gas, σ_s is the surface tension, γ_s is the surface curvature energy (c.f. Table I), and V is a mesoscopic electron-shell correction. The mode stiffness $\alpha(q; R_0, T)$ has the

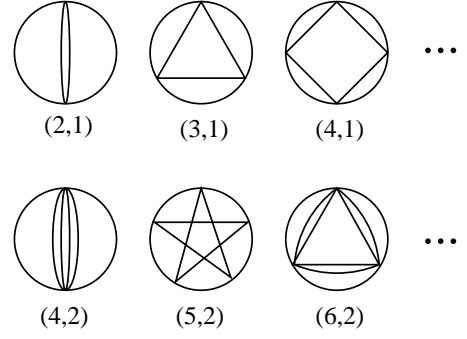


FIG. 2: Classical periodic orbits^{27,36} of an electron in a plane perpendicular to the axis of the wire, labeled (v, w) , where v is the number of vertices and w is the winding number.

following form²⁵ in the semiclassical approximation, valid for long-wavelength perturbations:

$$\alpha(q; R, T) = -2\pi\sigma_s/R + 2\pi(\sigma_s R - \gamma_s)q^2 + \left(\frac{\partial^2}{\partial R^2} - \frac{1}{R} \frac{\partial}{\partial R}\right) V(R, T), \quad (5)$$

where

$$V(R, T) = \frac{2\varepsilon_F}{\pi} \sum_{w=1}^{\infty} \sum_{v=2w}^{\infty} \frac{a_{vw}(T) f_{vw}}{v^2 L_{vw}} \cos(k_F L_{vw} - 3v\pi/2). \quad (6)$$

The sum in Eq. (6) includes all classical periodic orbits (v, w) in a disk billiard (see Fig. 2). $L_{vw} = 2vR \sin(\pi w/v)$ is the length of an orbit, the factor $f_{vw} = 1$ for $v = 2w$, 2 otherwise, accounts for the invariance under time-reversal symmetry of some orbits, and $a_{vw}(T) = \tau_{vw}/\sinh \tau_{vw}$ ($\tau_{vw} = \pi k_F L_{vw} T/2T_F$) is a temperature-dependent damping factor.^{27,36}

Since $\partial^2 \alpha / \partial q^2 > 0$ for all physically meaningful radii, long-wavelength perturbations cost the least energy,³⁷ and the stability of the wire is determined by the sign of $A(R_0, T) \equiv \alpha(q = 0; R_0, T)$. For $A(R_0, T) > 0$, a nanowire is stable with respect to all small perturbations, and is hence a metastable thermodynamic state. For $A(R_0, T) < 0$, the nanowire is unstable. The stability diagram so determined is shown in Fig. 1. In Fig. 1, the values $\sigma_s = \sigma_s(\text{FEM})$ and $\gamma_s = \gamma_s(\text{FEM})$, appropriate for alkali metals, were used (c.f. Table I). For larger values of σ_s (e.g. for noble metals), the maximum temperatures (in units of T_F) of the stable fingers are reduced somewhat, but the stability diagram is qualitatively similar.

Further insight into the stability criterion $A > 0$ is provided by the identity

$$A(R_0, T) = \left(\frac{\partial^2}{\partial R_0^2} - \frac{1}{R_0} \frac{\partial}{\partial R_0}\right) \frac{U_0(R_0, T)}{L}. \quad (7)$$

The wire can lower its potential energy via a volume-conserving separation into thicker and thinner segments

if and only if $A < 0$. $A < 0$ thus corresponds to an *inhomogeneous* phase, while $A > 0$ corresponds to a *homogeneous* phase.

Our analysis of stability in terms of the convexity of the constrained energy functional is quite different from simply comparing the energy of cylinders of different radius,^{22,29,38} which does not address the fundamental question: *whether any cylinder is stable*. We also point out that for a sufficiently large system, the number of atoms is conserved—neglecting sublimation—and the depletion of atoms from a finite segment of wire³⁸ can be described as a finite-wavelength perturbation of a larger system.

Note that our stability analysis is carried out at fixed L . The tensile force necessary to fix the length of the wire is given by $F = -\partial U_0/\partial L$ [plus a small correction due to surface fluctuations, c.f. Eq. (22)], and was previously calculated as a function of radius in this model in Refs. 9,10,30. Our stability analysis is thus appropriate to describe nanowires under tensile stress, such as those studied in the experiments of Refs. 11,12,13,14,15,16,17,18. The stability of a nanowire with free ends is an open question.

IV. LINEARIZED SURFACE DYNAMICS

A. Surface phonons

We first consider inertial dynamics of the ionic background. Assuming that the ionic medium is irrotational and incompressible,³⁹ its velocity distribution $\vec{v}(\vec{r}, t)$ can be written in terms of a potential satisfying the Laplace equation

$$\nabla^2 \Phi(\vec{r}, t) = 0, \quad (8)$$

where $\vec{v}(\vec{r}, t) = -\nabla \Phi(\vec{r}, t)$. The general solution to this equation with axial symmetry, which is regular at $r = 0$, can be written⁴

$$\Phi(\vec{r}, t) = \Phi(r, z, t) = \sum_{n=-N}^N d(q_n, t) I_0(q_n r) e^{iq_n z}, \quad (9)$$

where I_0 is the modified Bessel function of order zero and r is the distance of an ion from the z -axis.

For small deformations, the relation between the coefficients $d(q_n, t)$ in the expansion (9) and the Fourier coefficients $b(q_n, t)$ of the surface perturbation (1) can be determined by the condition that the radial component of the velocity at the surface is

$$v_r = -\frac{\partial \Phi(r, z, t)}{\partial r} \Big|_{r=R_0} = \frac{\partial R(z, t)}{\partial t} \quad (10)$$

plus terms $\mathcal{O}(b^3)$. Therefore, we have

$$d(q_n, t) = -\frac{1}{q_n I_1(q_n R_0)} \frac{\partial b(q_n, t)}{\partial t}, \quad (11)$$

where I_1 is the first-order modified Bessel function. The kinetic energy of the ionic medium is then given by

$$\begin{aligned} K &= \frac{\rho_i}{2} \int d^3 r \nabla \Phi^*(\vec{r}, t) \cdot \nabla \Phi(\vec{r}, t) \\ &= L \sum_{n=1}^N m(q_n, R_0) \left| \frac{\partial b(q_n, t)}{\partial t} \right|^2, \end{aligned} \quad (12)$$

where ρ_i is the ionic mass density, and

$$m(q, R) = \rho_i \frac{2\pi R I_0(qR)}{q I_1(qR)}. \quad (13)$$

Details of the derivation of Eqs. (12) and (13) are given in Appendix A. Combining Eqs. (3) and (12) yields a Hamiltonian for surface phonons, with frequencies

$$\omega(q; R_0, T) = \sqrt{\frac{\alpha(q; R_0, T)}{m(q, R_0)}}. \quad (14)$$

Generically, $\omega(q) \propto q$ as $q \rightarrow 0$ due to the q -dependence of $m(q, R_0)$. Eq. (14) thus describes *acoustic surface phonons*. On the stability boundary $A = 0$, one has $\omega(q) \propto q^2$ as $q \rightarrow 0$. For $A < 0$, ω is imaginary, and long-wavelength modes grow exponentially [see Fig. 5(a)].

B. Surface diffusion

The surface deformation (1) also produces a gradient in chemical potential that drives the surface atoms to diffuse—a process likely to be important for large-scale deformations.³⁵ The surface current of atoms is given by Fick's law

$$\vec{J} = -\frac{\rho_s D_s}{k_B T} \nabla \mu, \quad (15)$$

where ρ_s is the surface density of atoms and D_s is the surface self-diffusion constant. Using the continuity equation for the surface current, Eq. (15) can be converted into a (linearized) equation of motion for the profile $R(z, t)$

$$\frac{\partial R(z, t)}{\partial t} = \frac{\rho_s D_s v_a}{k_B T} \frac{\partial^2 \mu}{\partial z^2}, \quad (16)$$

where $v_a = 3\pi^2/k_F^3$ is the volume of an atom. The chemical potential μ of an atom is obtained by calculating the change in free energy with the addition of an atom at point z_0 ,

$$\mu(z_0, t) = U[R(z, t) + C\delta(z - z_0)] - U[R(z, t)], \quad (17)$$

where $C = v_a/2\pi R$ is chosen so that the volume of an atom is added. From Eq. (3), one obtains

$$\mu(z, t) = \mu_0 + \frac{\varepsilon_F v_a}{\pi R_0} \sum_{n=-N}^N \alpha(q_n; R_0, T) b(q_n, t) e^{iq_n z}, \quad (18)$$

where $\mu_0(R_0, T)$ is the chemical potential of the unperturbed cylinder. Combining Eqs. (16) and (18) yields an equation of motion for the Fourier component $b(q, t)$,

$$\frac{\partial b(q, t)}{\partial t} = -\Gamma(q; R_0, T)b(q, t), \quad (19)$$

where the relaxation rate

$$\Gamma(q; R_0, T) = \frac{\rho_s D_s v_a^2}{\pi R_0 k_B T} q^2 \alpha(q; R_0, T). \quad (20)$$

Thus, one finds that under surface diffusion alone, a perturbed metastable wire relaxes exponentially toward a cylindrical shape. For $\alpha < 0$, the mode grows exponentially.

C. Combined dynamics

Combining inertial and diffusive processes, the linearized (classical) equation of motion for the surface modes is

$$\frac{\partial^2 b(q, t)}{\partial t^2} + \Gamma(q) \frac{\partial b(q, t)}{\partial t} + \omega^2(q) b(q, t) = 0. \quad (21)$$

From the q -dependence of Eqs. (14) and (20), one sees that $\Gamma(q)/\omega(q) \rightarrow 0$ as $q \rightarrow 0$, indicating that diffusive processes can be neglected in this limit, at least for small deformations. In general, the relative time scales for inertial and diffusive dynamics depend on the value of D_s . For this quasi-one-dimensional diffusion problem, one can estimate $D_s \sim (\omega_D/\rho_s) \exp(-E_s/k_B T)$, where ω_D is the Debye frequency and E_s is the activation energy for surface diffusion, which is comparable to the energy of a single bond in the solid. With this estimate, one has $\omega(q) \gg \Gamma(q)$ for all q , indicating that the surface phonons are underdamped.

The picture of the surface dynamics of (meta)stable metal nanowires which emerges from this analysis is that there is a separation of timescales: on short timescales, the surface oscillates rapidly about the cylindrical equilibrium shape, while on much longer timescales, surface atoms diffuse irreversibly.

V. CRITICAL SURFACE FLUCTUATIONS

In the harmonic approximation [Eqs. (3) and (12)], the total free energy $\Omega(R_0, T)$ of the nanowire is given by the free energy of the unperturbed cylinder plus the Helmholtz free energy of the surface phonons,

$$\Omega = U_0 + \sum_{n=1}^N [\hbar \omega_n + 2k_B T \ln(1 - e^{-\beta \hbar \omega_n})], \quad (22)$$

where $\omega_n \equiv \omega(q_n; R_0, T)$ and $\beta = 1/k_B T$. The equilibrium tension in the wire is

$$F = -\frac{\partial \Omega}{\partial L} = -\frac{\partial U_0}{\partial L} + \delta F_{\text{phonon}}, \quad (23)$$

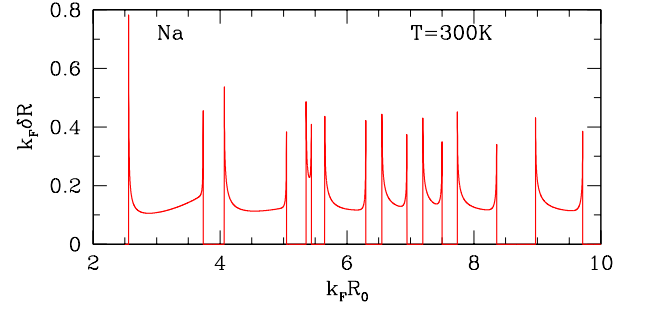


FIG. 3: Root-mean-square fluctuations of the radius of metastable sodium nanowires of length $L = 10R_0$. δR is undefined for unstable wires within the harmonic approximation, and is not shown.

where the main contribution $-\partial U_0/\partial L$ was previously calculated in Refs. 9,10,30, and δF_{phonon} is a small correction that is singular at the stability boundaries, where the surface modes become soft.

The softening of the surface modes on the stability boundaries leads to critical surface fluctuations. Given the stiffness (5) and frequency (14) of the surface modes, the mean-square thermal fluctuation δR^2 of the radius of the nanowire can be calculated in the usual way⁴⁰

$$\delta R^2 \equiv \langle (R - R_0)^2 \rangle = \frac{1}{L} \sum_{n=1}^N \frac{\hbar \omega_n [2f(\omega_n) + 1]}{\alpha(q_n; R_0, T)}, \quad (24)$$

where $f(\omega) = [\exp(\beta \hbar \omega) - 1]^{-1}$ is the Planck distribution. Note that, aside from a small quantum correction, the magnitude of the surface fluctuations follows from the equipartition theorem applied to Eq. (3), and is thus largely independent of the nature of the surface dynamics—whether inertial or diffusive.

Fig. 3 shows δR for nanowires of finite length at room temperature as a function of their mean radius. The ionic mass and Fermi temperature were taken to be that of sodium. Within a metastable region, $k_F \delta R \ll 1$ and is approximately independent of L , indicating that such wires are nearly atomically smooth at this temperature. The zero-point motion contributes roughly fifty percent of the surface fluctuation within a stable region for sodium nanowires at $T = 300K$. With increasing temperature, the thermal contribution to δR grows proportional to \sqrt{T} , according to the equipartition theorem. Note that the harmonic approximation is expected to break down when $k_F \delta R \sim 1$.

The surface fluctuation δR exhibits sharp peaks at the stability boundaries, reaching the value

$$\delta R^2|_{A(R_0, T)=0} = \frac{k_B T}{4\pi^3(\sigma R_0 - \gamma)} L, \quad (25)$$

plus a small quantum correction. δR thus scales as $L^{1/2}$ on the stability boundary, like the finite-size scaling at the roughening transition of a planar interface.⁴¹ At $T = 0$, δR remains small and approximately independent of L

on the stability boundary. The absence of critical surface fluctuations at $T = 0$ is also consistent with the behavior of planar interfaces.⁴⁰

The stability boundary $A(R_0, T) = 0$ defines a (multiple-valued) critical temperature $T_c = T_c(R_0)$ as a function of the mean radius, or alternatively a critical mean radius $R_c = R_c(T)$ as a function of temperature (see Fig. 1). Within the harmonic approximation, δR grows with an exponent $\nu = -1/4$ as $R_0 \rightarrow R_c$ or $T \rightarrow T_c$, as expected from the Ornstein-Zernicke fluctuation theory. This critical behavior, which is cut off when δR approaches the value given in Eq. (25), is illustrated in Fig. 3.

One can also study the time-dependence⁴² of δR for an initially cylindrical wire undergoing thermal fluctuations. Using the classical equipartition theorem, for each mode we have

$$\langle |b(q_n, t)|^2 \rangle = \frac{2k_B T}{L} \frac{\sin^2(\omega_n t)}{\alpha(q_n; R_0, T)} \quad (26)$$

where $\sin^2(\omega_n t)$ describes the standing capillary waves. The surface fluctuations then grow as a function of time according to

$$\delta R^2(t) = \frac{4k_B T}{L} \sum_{n=1}^N \frac{\sin^2(\omega_n t)}{\alpha(q_n; R_0, T)}. \quad (27)$$

On the stability boundaries $A(R_0, T) = 0$, the dispersion relation $\omega(q) \sim q^2$, and one finds asymptotically $\delta R(t) \sim t^{1/4}$ for times $\omega_1^{-1} \gg t \gg \omega_N^{-1}$. The dynamic exponent $z = 1/4$ differs from that of a planar interface⁴² due to the different dispersion relation for the surface modes.

However, all these scaling relations hold only in a limited range, since the asymptotic limit $\delta R \rightarrow \infty$ characterizing the roughening transition^{40,41,42} is unphysical in nanowires, due to their finite radius. On the stability boundary, the surface does not *roughen* in a thermodynamic sense, but the nanowire does become inhomogeneous.

VI. REENTRANT BEHAVIOR

Perhaps most interesting is the *reentrant* behavior occurring on the arches and overhangs in the stability diagram, Fig. 1. For instance, a wire with $k_F R_0 = 19$ is metastable and homogeneous in the temperature interval $T_{c1} < T < T_{c2}$, with $T_{c1} \approx .0072T_F$ and $T_{c2} \approx .046T_F$. The surface exhibits critical fluctuations as $T \rightarrow T_{c1}^+$ or $T \rightarrow T_{c2}^-$, at which points the wire makes a transition to an inhomogeneous phase. The transition at T_{c2} is conventional, in the sense that the inhomogeneous phase is the high-entropy phase. However, the inhomogeneous phase below T_{c1} has *lower entropy* than the homogeneous phase above T_{c1} . Fig. 4(a) shows the total entropy $S = -\partial\Omega/\partial T$ of the nanowire as a function of temperature, including both electron and phonon contributions,

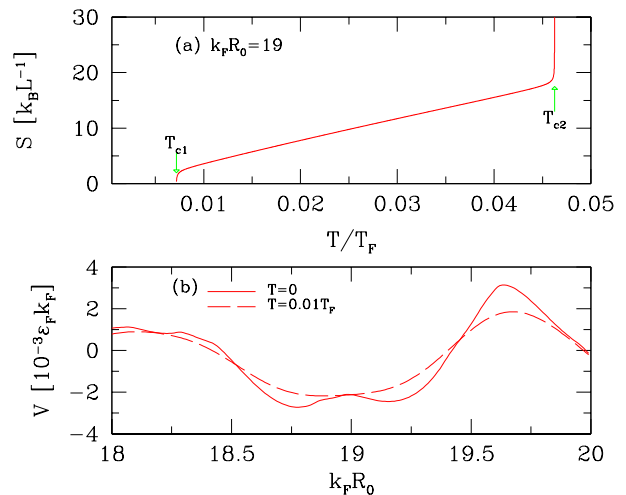


FIG. 4: (a) The total entropy per unit length of a nanowire with $k_F R_0 = 19$ versus temperature. The ionic mass was taken to be that of sodium. (b) The electron-shell potential $V(R_0, T)$, from Eq. (6).

where Ω is given by Eq. (22). The electronic entropy is regular at the critical points, but the phonon entropy is singular in the harmonic approximation, due to the emergence of soft surface modes. The singular contribution to the phonon entropy is

$$S_{\text{sing}}(R_0, T) = -\frac{\hbar}{L} \sum_{n=1}^N f(\omega_n) \frac{\partial \omega(q_n; R_0, T)}{\partial T}, \quad (28)$$

indicating that the softening of a phonon mode with decreasing temperature indeed leads to a decrease in entropy.

To understand the counterintuitive behavior at T_{c1} , it is useful to consider the electron-shell correction V to the energy of the wire, shown in Fig. 4(b). Above T_{c1} , V has a single broad minimum near $k_F R_0 = 19$, but as the temperature is lowered, and the fine structure in the shell potential emerges, this single minimum splits into two minima at $k_F R_0 = 18.75$ and $k_F R_0 = 19.2$. To lower its free energy, the system would like to fall into one of these two minima, but due to volume conservation, such a global change is not possible. The wire thus undergoes phase separation into thick and thin segments.³⁵

VII. UNSTABLE WIRES

Finally, let us discuss the dynamics of unstable wires. Fig. 5(a) shows the real and imaginary parts of the surface phonon frequency versus wavevector for a typical unstable wire. One mode $b(q_m, t)$ grows exponentially faster than all others in the harmonic approximation, and thus may be expected to dominate. For a single Fourier component $b(q_m)$, the potential energy $U[b(q_m)]$ of the nanowire can be evaluated for arbitrarily large b using

semiclassical perturbation theory. U may be expanded semiclassically as^{9,27}

$$U = u\mathcal{V} + \sigma_s\mathcal{S} - \gamma_s\mathcal{C} + \delta U. \quad (29)$$

The volume \mathcal{V} , surface area \mathcal{S} , and integrated mean curvature \mathcal{C} of the nanowire can be calculated for arbitrary

deformations by simple geometric considerations. Using semiclassical perturbation theory,^{43,44,45} the electron-shell correction δU can again be expressed in terms of the classical periodic orbits of a disk billiard, leading to an expression similar to Eq. (6):

$$\frac{\delta U[b(q_m)]}{L} = \frac{2\varepsilon_F}{\pi} \sum_{w=1}^{\infty} \sum_{v=2w}^{\infty} \frac{a_{vw}(T)f_{vw}}{v^2 L_{vw}} \left[\left(1 + \frac{b(0)}{R_0}\right) \cos(\theta_{vw}) J_0(\phi_{vw}) - \frac{2b(q_m)}{R_0} \sin(\theta_{vw}) J_1(\phi_{vw}) \right], \quad (30)$$

where $\theta_{vw} = k_F L_{vw}(1 + b(0)/R_0) - 3v\pi/2$, $\phi_{vw} = 2k_F L_{vw} b(q_m)/R_0$, J_i is the i -th order Bessel function, and $b(0)$ is related to $b(q_m)$ by Eq. (2). The result is shown in Fig. 5(b). Although the wire is unstable to breakup under a hypothetical long-wavelength perturbation, the energy of the fastest growing mode reaches a minimum at a finite amplitude, suggesting that the surface deformation *saturates*, and that the wire does not break up, but rather necks down to the next stable radius. A similar scenario is predicted under the diffusive dynamics of Eq. (19). An explicit nonlinear dynamical simulation³⁵ confirms these predictions.

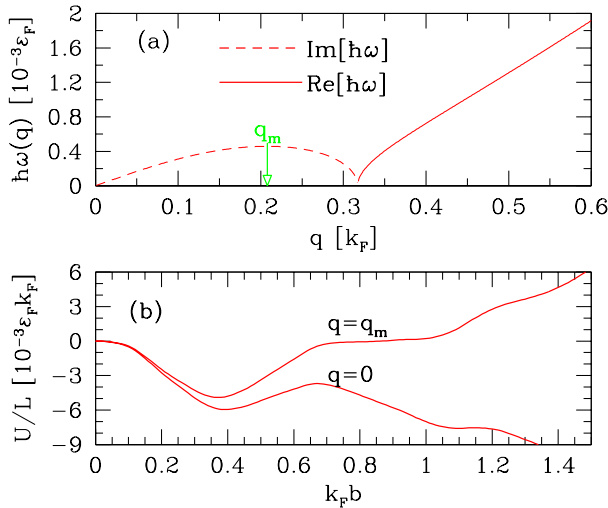


FIG. 5: (a) The dispersion relation for the surface modes of an unstable nanowire with $k_F R_0 = 8.95$ at $T = 0$. The ionic mass was taken to be that of sodium. (b) The potential energy $U[b(q)]$ of the same nanowire for sinusoidal deformations with $q = 0$ and $q = q_m = 0.208k_F$, respectively. Note that the energy U_0 of a straight wire has been subtracted. The different energies of these two modes is mainly due to the increased surface energy at finite q .

VIII. CONCLUSIONS

The stability and surface dynamics of metal nanowires were investigated in a continuum approach, including electron-shell effects. A thermodynamic phase diagram for jellium nanowires was derived, which predicts that cylindrical wires with certain “magic” conductance values are stable with respect to small perturbations up to remarkably high temperatures. On the stability boundary, the surface exhibits critical fluctuations, and the nanowire becomes inhomogeneous. Both surface phonons and surface self-diffusion of atoms were included in the linearized surface dynamics. It was found that inertial dynamics (phonons) always dominate the long-wavelength behavior, including the critical points. (It must be emphasized, however, that this conclusion holds only for *small* perturbations of the surface. The irreversible diffusion of surface atoms is undoubtedly crucial for large-scale surface deformations.³⁵) A novel reentrant behavior was predicted, in which a straight wire is stabilized at intermediate temperatures, but undergoes phase separation into thick and thin segments as the temperature is lowered. Finally, for unstable wires, the surface deformation was found to grow exponentially, dominated by a single Fourier component, and to saturate at a finite amplitude, indicating that unstable wires may not break, but rather neck down to the next stable radius.

The results presented in this article should be directly relevant for nanowires made of monovalent metals, especially the alkali metals and gold, for which there is clear experimental evidence of electron-shell effects.^{15,16,18} Moreover, this simple model may provide qualitative insight into the *generic* surface properties of metal nanowires, which could guide investigations of more realistic, material-specific models.

Acknowledgments

We acknowledge fruitful discussions with J. Bürki and R. Goldstein. CHZ and CAS were supported by NSF grants DMR0072703 and DMR0312028. This research

was supported by an award from Research Corporation.

APPENDIX A: THE IONIC KINETIC ENERGY

Here we present some details of the derivation of the expression (12) for the kinetic energy of the ions. Inserting Eq. (9) into the first line of Eq. (12) and performing the z -integral, one obtains

$$K = \pi \rho_i L \sum_n \int_0^{R_0} r dr [q_n^2 I_0'^2(q_n r) + q_n^2 I_0^2(q_n r)] |d(q_n, t)|^2. \quad (\text{A1})$$

Using the relation $I_0'(x) = I_1(x)$ and the identity

$$\frac{d}{dx} [x I_m(x) I_m'(x)] = x \left[I_m'^2 + \left(1 + \frac{m^2}{x^2}\right) I_m^2 \right], \quad (\text{A2})$$

the radial integral in Eq. (A1) may be performed, leading to the result

$$K = \pi \rho_i L \sum_{n=-N}^N q_n R_0 I_0(q_n R_0) I_1(q_n R_0) |d(q_n)|^2. \quad (\text{A3})$$

Finally, eliminating $d(q_n, t)$ from Eq. (A3) using the relation (11), one obtains the second line of Eq. (12).

-
- ¹ *International Technology Roadmap for Semiconductors*, <http://public.itrs.net/> (Semiconductor Industry Association, 2001).
 - ² G. E. Moore, *Electronics* **38**(8) (1965).
 - ³ C. Dekker, *Phys. Today* **52**, 22 (1999), and references therein.
 - ⁴ S. Chandrasekhar, *Hydrodynamic and Hydromagnetic Stability*, (Dover, New York, 1981), pp. 515-74.
 - ⁵ J. Plateau, *Statique expérimentale et théorique des liquides soumis aux seules forces moléculaires*, (Gautier-Villars, Paris, 1873).
 - ⁶ R. B. Ross, *Metallic Materials Specification Handbook*, 4th Ed. (Chapman and Hall, London, 1992).
 - ⁷ W. R. Tyson and W. A. Miller, *Surf. Sci.* **62**, 267 (1977).
 - ⁸ J. P. Perdew, Y. Wang, and E. Engel, *Phys. Rev. Lett.* **66**, 508 (1991).
 - ⁹ C. A. Stafford, F. Kassubek, J. Bürki, and H. Grabert, *Phys. Rev. Lett.* **83**, 4836 (1999).
 - ¹⁰ C. A. Stafford, F. Kassubek, J. Bürki, H. Grabert, and D. Baeriswyl, in *Quantum Physics at the Mesoscopic Scale*, D. C. Glatli, M. Sanquer, and J. Tran Thanh Van eds. (EDP Sciences, Les Ulis, France, 2000), pp. 445-449.
 - ¹¹ C. Rubio, N. Agraït, and S. Vieira, *Phys. Rev. Lett.* **76**, 2302 (1996).
 - ¹² C. Untiedt, G. Rubio, S. Vieira, and N. Agraït, *Phys. Rev. B* **56**, 2154 (1997).
 - ¹³ Y. Kondo and K. Takayanagi, *Phys. Rev. Lett.* **79**, 3455 (1997); *Science* **289**, 606 (2000).
 - ¹⁴ H. Ohnishi, Y. Kondo, and K. Takayanagi, *Nature* **395**, 780 (1999); A. I. Yanson, G. Rubio Bollinger H. E. van den Brom, N. Agraït, and J. M. van Ruitenbeek, *ibid.* **395**, 783 (1999).
 - ¹⁵ A. I. Yanson, I. K. Yanson, and J. M. van Ruitenbeek, *Nature* **400**, 144 (1999); *Phys. Rev. Lett.* **84**, 5832 (2000).
 - ¹⁶ A. I. Yanson, I. K. Yanson, and J. M. van Ruitenbeek, *Phys. Rev. Lett.* **87**, 216805 (2001); *Low Temp. Phys.* **27**, 807 (2001).
 - ¹⁷ V. Rodrigues, J. Bettini, A. R. Rocha, L. G. C. Rego, and D. Ugarte, *Phys. Rev. B* **65**, 153402 (2002).
 - ¹⁸ M. Diaz, J. L. Costa-Kramer, E. Medina, A. Hasmy, and P. A. Serena, *Nanotechnology* **14**, 113 (2003).
 - ¹⁹ U. Landman, W. D. Luedtke, N. A. Burnham, and R. J. Colton, *Science* **248**, 454 (1990).
 - ²⁰ T. N. Todorov and A. P. Sutton, *Phys. Rev. B* **54**, R14234 (1996).
 - ²¹ M. R. Sørensen, M. Brandbyge, and K. W. Jacobsen, *Phys. Rev. B* **57**, 3283 (1998).
 - ²² O. Gülseren, F. Ercolessi, and E. Tosatti, *Phys. Rev. Lett.* **80**, 3775 (1998).
 - ²³ G. Bilalbegović, *Phys. Rev. B* **58**, 15412 (1998).
 - ²⁴ B. Wang *et al.* *Phys. Rev. Lett.* **86**, 2046 (2001).
 - ²⁵ F. Kassubek, C. A. Stafford, H. Grabert, and R. E. Goldstein, *Nonlinearity* **14**, 167 (2001).
 - ²⁶ An analysis of the *lifetime* of these metastable states would be necessary to fully address this issue.
 - ²⁷ M. Brack and R. K. Bhaduri, *Semiclassical Physics*, (Addison-Wesley, Reading, MA, 1997).
 - ²⁸ C. Yannouleas, E. N. Bogachev, and U. Landman, *Phys. Rev. B* **57**, 4872 (1998).
 - ²⁹ M. J. Puska, E. Ogando, and N. Zabala, *Phys. Rev. B* **64**, 033401 (2001).
 - ³⁰ C. A. Stafford, D. Baeriswyl, and J. Bürki, *Phys. Rev. Lett.* **79**, 2863 (1997).
 - ³¹ W. A. de Heer, *Rev. Mod. Phys.* **65**, 611 (1993); M. Brack, *ibid.* **65**, 677 (1993).
 - ³² J. Bürki, C. A. Stafford, X. Zotos, and D. Baeriswyl, *Phys. Rev. B* **60**, 5000 (1999); *Phys. Rev. B* **62**, 2956 (2000).
 - ³³ J. Bürki and C. A. Stafford, *Phys. Rev. Lett.* **83**, 3342 (1999).
 - ³⁴ R. H. M. Smit, C. Untiedt, A. I. Yanson, and J. M. van Ruitenbeek, *Phys. Rev. Lett.* **87**, 266102 (2001).
 - ³⁵ J. Bürki, R. E. Goldstein, and C. A. Stafford, *cond-mat/0208540*.
 - ³⁶ R. Balian and C. Bloch, *Ann. Phys. NY* **69**, 76 (1972).
 - ³⁷ A short-wavelength Peierls instability also arises in a fully quantum-mechanical treatment (D. F. Urban and H. Grabert, *cond-mat/0307279*), but only in very long wires at low temperatures.
 - ³⁸ E. Tosatti, S. Prestipino, S. Kostlmeier, A. Dal Corso, and F. D. Di Tolla, *Science* **291**, 288 (2001).
 - ³⁹ A similar assumption was employed to study the vibrational spectrum of metal clusters by C. Yannouleas and U. Landman, *J. Phys. Chem. A* **102**, 2505 (1998).
 - ⁴⁰ D. S. Fisher and J. D. Weeks, *Phys. Rev. Lett.* **50**, 1077 (1983).
 - ⁴¹ M. E. Fisher, *J. Chem. Soc. Faraday Trans. 2* **82**, 1569 (1986).
 - ⁴² E. G. Flekkøy and D. H. Rothman, *Phys. Rev. Lett.* **75**, 260 (1995).
 - ⁴³ D. Ullmo, M. Grinberg, and S. Tomsovic, *Phys. Rev. E* **54**,

136 (1996).

⁴⁴ S. C. Creagh, Ann. Phys. **248**, 60 (1996).

⁴⁵ C. A. Stafford, F. Kassubek, and H. Grabert, in *Ad-*

vances in Solid State Physics, Volume 41, B. Kramer ed. (Springer-Verlag, Berlin Heidelberg, 2001), pp. 497–511.